The Journal of Experimental Biology 212, 2491-2499
Published by The Company of Biologists 2009
doi:10.1242/jeb.025767

A dynamic model of the windlass mechanism of the foot: evidence for early stance phase preloading of the plantar aponeurosis

Paolo Caravaggi[1,*], Todd Pataky[1], John Y. Goulermas[2], Russel Savage[1] and Robin Crompton[1]

[1]HACB, School of Biomedical Sciences, University of Liverpool, Sherrington Buildings, Liverpool L69 3GE, UK and [2]Department of Electrical Engineering and Electronics, University of Liverpool, Liverpool L69 3BX, UK

*Author for correspondence (e-mail: pacara@liv.ac.uk)

Accepted 26 April 2009

SUMMARY

In the present study we have estimated the temporal elongation of the plantar aponeurosis (PA) during normal walking using a subject-specific multi-segment rigid-body model of the foot. As previous studies have suggested that muscular forces at the ankle can pre-load the PA prior to heel-strike, the main purpose of the current study was to test, through modelling, whether there is any tension present in the PA during early stance phase. Reflective markers were attached to bony landmarks to track the kinematics of the calcaneus, metatarsus and toes during barefoot walking. Ultrasonography measurements were performed on three subjects to determine both the location of the origin of the PA on the plantar aspect of the calcaneus, and the radii of the metatarsal heads. Starting with the foot in a neutral, unloaded position, inverse kinematics allowed calculation of the tension in the five slips of the PA during the whole duration of the stance phase. The results show that the PA experienced tension significantly above rest during early stance phase in all subjects (P<0.01), thus providing support for the PA-preloading hypothesis. The amount of preloading and the maximum elongation of the slips of the PA decreased from medial to lateral. The mean maximum tension exerted by the PA was 1.5 BW (body weight) over the three subjects.

Supplementary material available online at http://jeb.biologists.org/cgi/content/full/212/15/2491/DC1

Key words: foot biomechanics, plantar aponeurosis, windlass mechanism, computer modelling, inverse kinematics.

INTRODUCTION

The dynamic action of the plantar aponeurosis (PA) is of great biomechanical interest as it represents, together with the long plantar ligament and the spring ligament, one of the main structures maintaining the integrity of the arch of the foot, which serves also as an important energy-storing mechanism (Ker et al., 1987). The PA is a strong elastic band spanning the foot longitudinally and connecting the calcaneus to the toes. It appears as a strong and thick band from the heel to midfoot, from which point it fans out into five slips that run underneath the metatarsal heads (MHs) and attach to the plantar side of the proximal phalanx of each toe. During dorsiflexion of the toes, as occurs in late stance, the PA is stretched as it wraps around the MH. This is the so-called windlass mechanism which, in the late phase of stance, is responsible for raising the arch of the foot (Hicks, 1954) and contributing to stiffening of the foot by pulling on the heel, causing inversion at the subtalar joint and 'locking' the midtarsal joint (Briggs and Tansey, 2001). Previous studies using finite elements (Cheung et al., 2004; Giddings et al., 2000) and mechanical models (Fuller, 2000; Gefen, 2003) have investigated the static biomechanics of this component but so far only one paper has addressed the dynamic behaviour of the PA, using cadaveric feet (Erdemir et al., 2004). We infer that the dynamics of the PA are intrinsically correlated to the kinematics of the segments to which it is attached and with the geometry, specifically the radius and dorsoventral dimension of the MHs. Moreover we postulate that the pronounced medial arch of the normal foot suggests that higher tension forces support the medial side and, given the PA is probably the main passive structure supporting the arch, that this is reflected in the distribution of the total longitudinal tension among its mediolateral slips. Therefore the model herein proposed aims to provide a non-invasive tool to test two main hypotheses: first that the PA is preloaded at heel-strike; and second that the geometry of the MHs and the mediolateral kinematic differences of the metatarsophalangeal joints (MTPJs) affect the longitudinal tension borne by the more medial and more lateral slips of the PA. To test these hypotheses we established a multi-body inverse-kinematic model of the windlass mechanism, built on anthropometric measurements of subjects and driven by *in vivo* kinematic data, able to evaluate the length *versus* time relationship of the slips of the PA segments for the duration of the stance phase of barefoot walking.

MATERIALS AND METHODS

Three subjects (age 27±7.8 years, weight 65.1±7.2 kg, height 1.78±0.15 m), with no history of lower limb major injuries or abnormalities, volunteered as subjects in this study, which used protocols approved by the Research Ethics Committee of The University of Liverpool.

Non-invasive ultrasound sonography was performed on the left foot of each subject in order to identify the origin of the PA and to estimate the radius of the MHs. Manual biometry was employed to record the main dimensions of the toes. Subsequently the subjects' feet were fitted with reflective markers using double-sided adhesive tape and kinematics were recorded at the subjects' (subjectively determined) normal walking speed when walking over a wooden walkway with an inset forceplate. The marker trajectories were filtered and imported into a multi-segment rigid-body model of the foot and inverse kinematic analysis was run to determine PA tension ($PA_{tension}$) trajectories for each trial recorded. These analyses used

Fig. 1. The plantar aponeurosis (PA) origin is located by placing the ultrasound probe on the sole of the foot, with the supporting plate kept firmly in place by an elastic band wrapped around the dorsum of the foot.

the anthropometric data from each subject and the kinematics of each trial to build subject-specific geometry and to compute PA elongation with time. Details of the method follow.

Sonography

Sonography was performed using a linear probe (Echo Blaster 128 EXT-1Z, Telemed, Vilnius, Lithuania) and settings suitable for superficial musculoskeletal structures (5 MHz; 50 mm depth; dynamic range, 56 dB). The linear probe was fixed perpendicular to a rigid plate on which a rectangular hole, the size of the probe sensor, had been made. The plate was aligned with the sole of the subject's foot and kept in position by an elastic band wrapped around the dorsum of the foot (Fig. 1). Sagittal imaging of the PA was then performed. The PA appeared as a white strip attached to the anterior aspect of the inferior border of the calcaneus; at each dorsiflexion apparent tensing was evident by slight changes in its orientation and by the PA becoming more parallel to the probe surface (Fig. 2). Once the PA origin (PA_o) had been identified and located approximately at the centre of the ultrasound image, the position of the probe was marked on the skin by passing the tip of a pen through two holes made on the plate, 1 cm on either side of the centre of the probe. The midpoint between these two points represents the projection of the origin of the PA onto the sole of the foot (PA_p). The depth (d) of the origin of the PA_o, that is the distance of the PA origin to the probe surface, was recorded (Fig. 2).

The probe, once removed from the supporting plate, was then placed on the plantar side of each MH and aligned with each (slightly flexed) toe. The curvature of the plantar surface of the MH can be seen clearly in Fig. 3. The cephalic radius of the MH can be approximated by a circle passing through three points on the curvature. Three different measurements, for a total of nine points, were taken for each MH. A Matlab routine (version 7.5, The MathWorks, Natick, MA, USA) then calculated the radius of the circle passing through each triplet of points; the radius of the given MH was taken as the average of the three measurements.

Stereophotogrammetry

Six motion-tracking cameras (ProReflex 1000 MCU, Qualysis, Gothenburg, Sweden) were used to track the kinematics of the foot during the stance phase of walking.

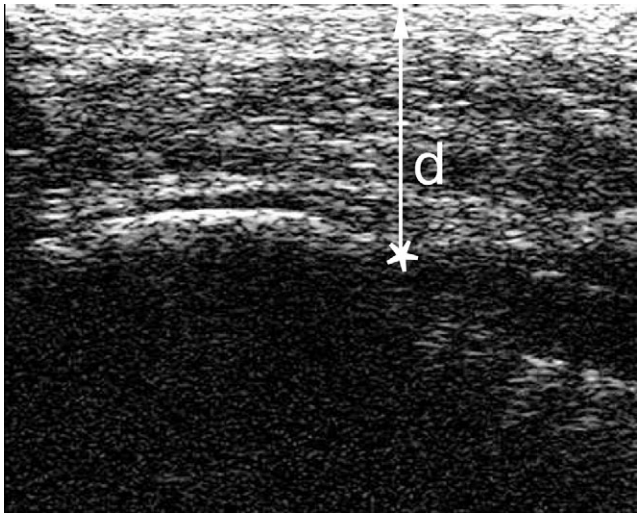

Fig. 2. Longitudinal sonography of the calcaneus of one of the subjects. The asterisk shows where the PA originates at the inferior border of the calcaneus. The depth (d) of the PA origin (PA_o) is measured as the distance from the asterisk to the top of the image, where the probe is in contact with the sole of the foot.

Ground reaction forces were recorded (forceplate model 9281C, Kistler Instruments, Hook, Hampshire, UK) and used to identify stance-phase timing. The subjects' left feet were fitted with 12 (7 mm diameter) reflective markers, attached using double-sided adhesive tape, to track the movement of the calcaneus, the metatarsus and the five toes (Table 1; Fig. 4). The marker set is essentially a modification of the protocol designed by Leardini and colleagues (Leardini et al., 2007), in which four markers were added to the heads of the proximal phalanges of toe 2 to 5. Although three non-collinear points are sufficient to track the movement of a rigid body in space, it was decided to track the movement of the metatarsus using four markers (FMH, FMB, VMH and VMB) as a rigid body assumption seemed inappropriate given the motion of the five metatarsals.

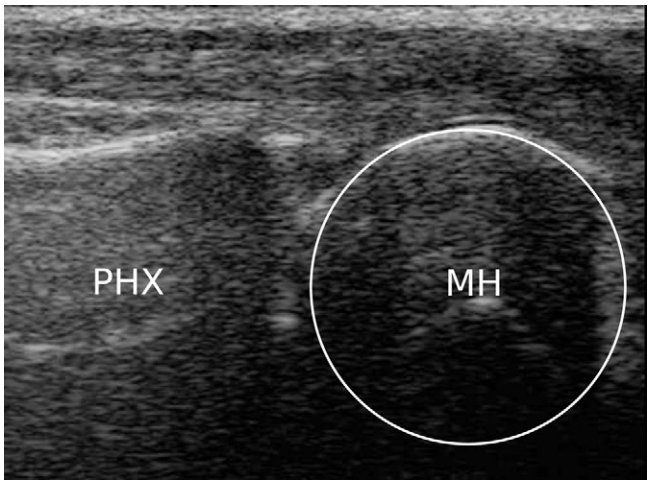

Fig. 3. The ultrasound probe placed longitudinally on the plantar side of the first metatarsophalangeal joint (MTPJ) shows the round profile of the metatarsal head (MH; right) and the inferior border of the proximal phalanx (PHX, left). The curvature of the MH can be approximated by a circle (in white).

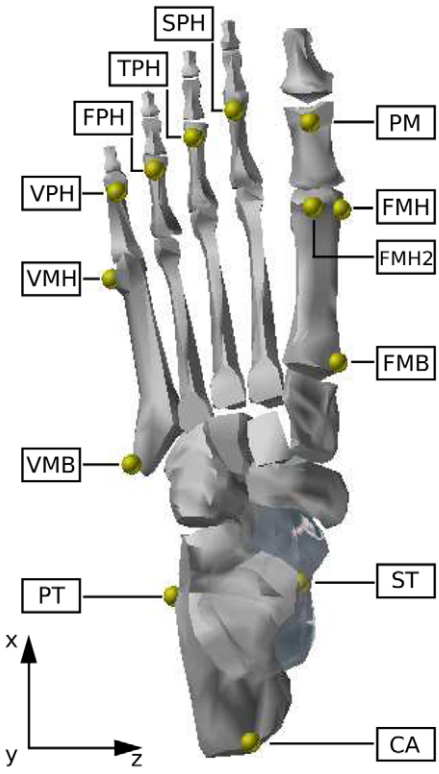

Fig. 4. A rendering of a foot model showing the location of the reflective markers (yellow spheres) used for this study and their acronyms. Bottom left is the global reference frame (lab reference). For definition of acronyms see Table 1.

A static calibration of the markers *in situ* was taken with the foot in neutral position on the ground. This posture was achieved by placing the target foot anterior to the contralateral foot so that the heel was approximately aligned to the contralateral first MTPJ. The subject shifted body weight so that it was carried primarily on the contralateral foot. In this position the knee of the instrumented foot was slightly flexed and the hip of the contralateral leg laterally tilted (Fig. 5). This position minimized the load borne by the foot, so that the PA would as far as possible be fully relaxed, while maintaining a quasi-normal body posture. In order to identify the sagittal plane of the hallux, and only for this static calibration, an additional marker (FMH2) was placed over the distalmost central point of the first metatarsal. This calibration allowed determination of the resting lengths of the PA slips, the MTPJ neutral (0 deg.) angles, and the location and orientation of the rigid-body segments at the start of the dynamic analysis.

Table 1. Table of acronyms and bony landmarks of the marker set used for this investigation

Marker acronym	Bony landmark
CA	Achilles' tendon attachment
ST	Sustentaculum tali
PT	Peroneal tubercle
FMH	First metatarsal head, most distal medial dorsal side
FMH2	First metatarsal head, most distal central dorsal side
FMB	First metatarsal base, most proximal medial dorsal side
VMH	Fifth metatarsal head, most distal lateral dorsal side
VMB	Fifth metatarsal base, most proximal lateral dorsal side
PM	Head of the proximal phalanx of the 1st toe, distal-most central dorsal point
SPH	Head of the proximal phalanx of the 2nd toe, distal-most central dorsal point
TPH	Head of the proximal phalanx of the 3rd toe, distal-most central dorsal point
FPH	Head of the proximal phalanx of the 4th toe, distal-most central dorsal point
VPH	Head of the proximal phalanx of the 5th toe, distal-most central dorsal point

See Fig. 4 to visualize the location of each marker on the foot.

Subsequently a reflective marker was placed on the sole of the foot at PA_p, the projection of PA_o on the sole of the foot. Another static calibration was made with the subject's foot suspended over the ground in such a way that the four reflective markers on the rearfoot could be imaged by the cameras. A Matlab routine was then used to calculate the 3D location of the PA_o on the calcaneus when the foot was on the ground in neutral position.

The three markers (CA, PT and ST) attached over the calcaneus defined a local reference system. If **A** is the (3×3) matrix of direction cosines specifying the orientation of the calcaneus with respect to the ground, and **B** that when in neutral position on the ground, it is possible to compute the rotation matrix **R** from **A** to **B** as:

$$\mathbf{R}_{\mathbf{B}}^{\mathbf{A}} = \mathbf{A}^{-1} \cdot \mathbf{B} \,. \quad (1)$$

Therefore, if $\mathbf{PA}_{\mathbf{p}}^{\mathbf{A}}$ is the (1×3) vector location of PA_p in **A**, we can write:

$$\mathbf{PA}_{\mathbf{p}}^{\mathbf{B}} = \mathbf{PA}_{\mathbf{p}}^{\mathbf{A}} \cdot \mathbf{R}_{\mathbf{B}}^{\mathbf{A}} \,, \quad (2)$$

where $\mathbf{PA}_{\mathbf{p}}^{\mathbf{B}}$ is the (1×3) vector location of PA_p in **B**.

PA_o can finally be established as:

$$\mathbf{PA}_{\mathbf{o}}^{\mathbf{B}} = \mathbf{PA}_{\mathbf{p}}^{\mathbf{B}} + \mathbf{d} + \underline{\mathbf{d}} \,, \quad (3)$$

where **d** and $\underline{\mathbf{d}}$ translate $\mathbf{PA}_{\mathbf{p}}^{\mathbf{B}}$ along the *y*-axis of the global reference frame: $|\mathbf{d}|=d$ is the depth of the PA origin as measured by sonography (Fig. 2), $\underline{\mathbf{d}}$ is a correction factor that takes into account soft tissue deformation (about 4 mm), as a consequence of the pressure exerted by the probe on the sole of the foot, and the radius of the reflective marker (3.5 mm). Marker motion was sampled at 250 Hz.

Fig. 5. One of the subjects standing with the left foot in neutral position. The position is achieved by shifting the body weight onto the right foot. The foot instrumented with markers is placed immediately anterior to the free one, while the leg is slightly flexed at the knee.

Manual biometry

The total length of each toe was measured as the distance between the most distal central point on the dorsal side of each metatarsal and tip of the toe; proximal phalanx length (*l*) as the distance between the former and the reflective marker on that toe. Phalanx width and thickness at the first interphalangeal joint were measured with calipers. These measurements were used to create toe geometry and to help locate the axis of rotation of the MTPJs.

Rigid body model

A commercial software package for multibody dynamic analysis (MSC.ADAMS Ver.2005.2.0, MSC Software Corporation, Santa Ana, CA, USA) was used to build the model geometry, which was customized for each subject's morphology. The size and position of the ellipsoids approximating the calcaneal and metatarsal segments were parameterized using the marker location with the foot in the neutral position. The toes were modelled according to the manual biometric measurements described above. The marker locations when the foot was in the neutral position and the sonographic measurements helped establish a reference frame for each MTPJ. The ellipsoid representing each toe was assumed to be parallel to the hallux, the longitudinal axis of which belonged to the sagittal plane through FMH2 and PM and intersected the origin of the MTPJ reference frame (Fig. 6).

As Briggs (Briggs, 2005) points out, the MTPJs are actually 'sloppy hinge joints' providing flexion/extension but also a small amount of abduction/adduction. Here they were modelled as ideal hinge joints, the rotation axis of which was assumed to be parallel to the *z*-axis and to pass through the origin of the MTPJ reference frame. This location and orientation were used as the estimated starting values for an optimization routine which determined the MTPJ centres and orientations. Just as is the case for many other joints in the human body, the MTPJ axis is not stationary. Therefore an optimization approach was chosen to compute the location and orientation of a 'compromise' axis at each MH, the mean of the momentary axes of rotation (see Appendix).

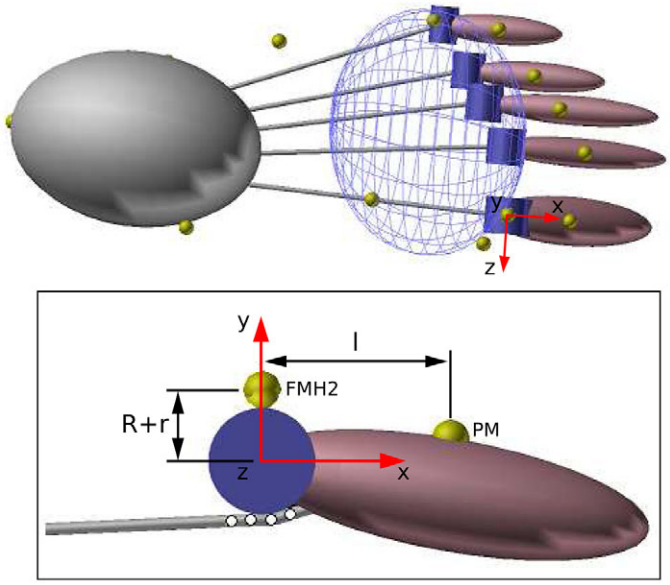

Fig. 6. Top: the multi-segment model in ADAMS (see text), for one of the three subjects, with the foot in the neutral starting position. The five slips of the PA attach to the calcaneus (grey ellipsoid) around PA_o and run longitudinally towards the inferior border of the proximal phalanx of each toe (in pink). The 12 yellow spheres are the 'motion agents', which drive the segments in the inverse kinematic analysis. The metatarsus is shown as a rigid ellipsoid. Bottom: detail of the first MTPJ. The PA slip inserts at the inferior border of the proximal phalanx and wraps around the MH (blue cylinder) through four small spherical contact elements. The MTPJ reference frame (in red) is located according to the biometric and sonographic measurements: *l* is the length of the proximal phalanx; *R* and *r* are the radii of the metatarsal head and of the reflective marker, respectively.

The five metatarsal bones are normally considered as a single unit in kinematics (Carson et al., 2001; Leardini et al., 2007) as there is little motion between the metatarsal bones. Referring to Fig. 6, the metatarsus is shown as a rigid ellipsoid, included only for visualization purposes. The actual interaction modelled was between the PA slips and the MHs represented as cylinders (which can be considered as moving rigidly with the metatarsus). The ultrasound measurements provided the radii for the cylinders approximating the MHs. The cylinders were set at the location of the MTPJ centre, with their longitudinal axis parallel to the *z*-axis of the MTPJ reference frame.

The PA was modelled as five springs, attached proximally to the calcaneus and distally to the inferior border of the proximal phalanx of each toe. More precisely the central spring was attached at PA_o and the origins of the other four springs were uniformly distributed around the central origin over a total width of 20 mm. In order to calculate the tension exerted by each slip of the PA, bulk stiffness values were assigned in accordance with Kitaoka et al. (Kitaoka et al., 1994), whose study showed little difference in the stiffness of different longitudinal bands of the PA from medial to lateral, any differences being dependent on the technique used to subdivide the PA more than on genuinely different zone-related material properties. Therefore, the mean stiffness value of 203.7 N mm^{-2} found in that study was divided by five, the number of longitudinal springs in parallel forming the PA structure.

Distally four small spheres allowed the elastic elements to wrap around the MH (Fig. 6); frictionless contact forces were created between the spheres and cylinders. These spheres simulate the action of the 'plantar plates', fibrocartilaginous plates which lie over the plantar aspect of the MTPJ. The fibre composition and orientation of these structures suggests that their main functions are to transmit the tensile load of the PA to the proximal phalanges and to sustain compressive weight, so supporting the articular surface of the MTPJ (Gregg et al., 2007; Mohana-Borges et al., 2003, see Fig. 7).

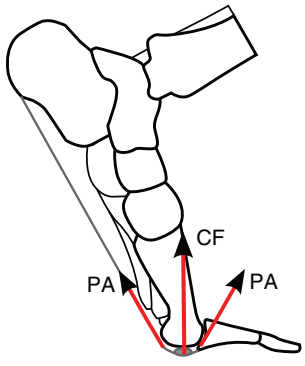

Fig. 7. Diagram of the internal forces between plantar aponeurosis and metatarsal head during late stance at one of the five MTPJs. PA is the tension in the plantar aponeurosis, CF is the contact force between the plantar aponeurosis and metatarsal head. The $PA_{tension}$ pulls at the insertion on the plantar plate and at the attachment to the proximal phalanx. The resultant is the contact force CF. The same force CF is applied by the metatarsal head downwards to the plantar plate.

Table 2. The cephalic radius (mm) of the five metatarsal heads (MH 1=medial; MH 5=lateral) for the three subjects

Metatarsal head	Subject 1	Subject 2	Subject 3	Mean±s.d.
MH 1	9.5±0.5	8.5±0.6	9.5±0.4	9.2±0.6
MH 2	7.7±0.9	6.4±0.5	8.4±0.3	7.5±1.0
MH 3	7.4±0.8	6.6±0.5	6.7±0.4	6.9±0.4
MH 4	6.6±0.2	6.2±0.4	7.3±0.6	6.7±0.6
MH 5	5.7±0.6	5.2±0.2	6.7±0.6	5.9±0.7

The means over three measurements are shown for each MH of each subject.

Anatomically the plantar plates provide insertions for the PA and are linked transversely by the deep transverse intermetatarsal ligaments (Briggs, 2005). The mediolateral stabilization action of these ligaments was simulated in the model by adding two elastic 'ligaments' to each side of the contact spheres. This allowed the PA slips to move backwards and forwards underneath each MTPJ while preventing them from losing contact with the MH during dynamic analysis. Fig. 6 shows the full model as created for one of the subjects used in this study.

Inverse kinematics

Following a residual analysis (Jackson, 1979), the trajectories of the reflective markers were filtered using a zero-phase-shifting low-pass filter, with a cut-off frequency of 12 Hz. Force plate timing information was used to select the range of data representing the stance phase. Model geometry was set for each subject according to the location of the twelve markers with the foot in a neutral position. For each set of walking kinematics the analysis was performed in two steps. First the foot segments were translated from their neutral positions to the first frame of the stance phase (heel-strike). This neutral position was the position of the segments at the start of the analysis (Fig. 5), guaranteeing that the PA 'springs' were fully relaxed before the inverse kinematic analysis was run. New trajectories were created through linear interpolation for each trial and each marker in order to get the segments into position for the second part of the analysis. Subsequently the temporal profiles of the marker trajectories, as recorded *in vivo*, were used to drive the segments in the actual inverse kinematic analysis of the stance phase. This two-step dynamic analysis was run for each trial of each subject (see supplementary material Movie 1). At the end of each analysis the deformation *versus* time curves of the five PA elastic slips, the contact forces between spheres and MH, and the MTPJ flexion/extension angles were exported for further scrutiny.

RESULTS

Ultrasonography permitted measurement of the depth of the PA origin, PA_o. The mean depth d of PA_o for the three subjects was 14.7±0.4 mm (mean±s.d.). The value of d was used, together with the location of PA_p relative to the reference frame of the calcaneus, to determine the 3D location of PA_o. The distance between PA_o and the insertion on the plantar side of the MH, when the foot is in neutral position, represented the resting lengths of each slip of the PA (Table 3). Furthermore, by applying linear ultrasound measurements to the plantar side of each MH, we were able to estimate the cephalic radius of the metatarsals in the parasaggital plane. The average radii of the five MHs as assessed by sonography are shown in Table 2.

Inverse kinematics allowed calculation of the temporal elongation/tension of the five slips of the PA during the normalized duration of the stance phase (Fig. 8). Mean intersubject walking speed over 15 trials was 1.59±0.05 m s^{-1} (mean±s.d.). Fig. 9 shows the means over five trials of the maximum elongation in each PA slip. The total tensional load in the PA was found to decrease from medial to lateral. The medial slip took up to 27% of the total load, the three central slips took about 19% of the total, and the lateral slip took the least tension, at about 15% of the total (Figs 8 and 9). A significant level of tension in the PA was present in all three subjects during early stance. One-sided single sample t-test of intersubject mean $PA_{tension}$, over the first 10% of normalized stance phase, compared with 0 (N) tension when PA was fully unloaded in neutral position confirmed the existence of early stance phase preloading ($PA_{tension}$=0.47±0.03 BW; P<0.01). Force plate measurements confirmed that the load borne by the subjects' feet, when in neutral position, was small (0.05±0.01 BW). In late stance the body weight is over the forefoot and the windlass mechanism will thus act to increase the tension in the PA through MTPJ dorsiflexion. Fig. 10 shows the intersubject temporal distribution of dorsiflexion angles of the MTPJs. The mean temporal profiles of MTPJ dorsiflexion angles at heel-strike and push-off for the three subjects are listed in Table 4. According to the current model the intersubject maximum $PA_{tension}$ at push-off was about 1.5 BW (Fig. 8). The plantar plates, which receive insertion from the PA, therefore exerted a vertical force on the MH as a consequence of the direction of 'pull' of $PA_{tension}$ (Fig. 7). Fig. 11 shows the intersubject mean curves, over 15 trials, of the resultant vertical contact forces applied to the MH by each PA slip, during the normalized stance phase. A good linear relationship (Eqn 4 and Fig. 12) was found between the maximum tension exerted in each PA slip ($PA_{tension}$) and the relative maximum vertical contact force (CF) applied to the MH (as %BW):

$$CF = 1.13 \times PA_{tension} - 0.1 , \quad (4)$$

(R^2=0.923; RMSE=0.03571).

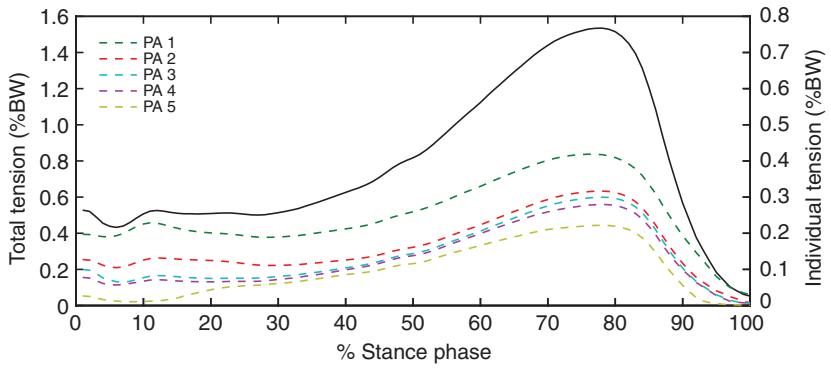

Fig. 8. Dashed curves represent the intersubject mean temporal profiles, over 15 trials, of the tension in each PA slip (PA 1=medial; PA 5=lateral) during normalized stance phase duration. The solid curve is the total tension in the PA, the sum of the tensions in each slip. Vertical axes of different scales have been employed to better visualize the individual tensions (right axis) and the total tension (left axis).

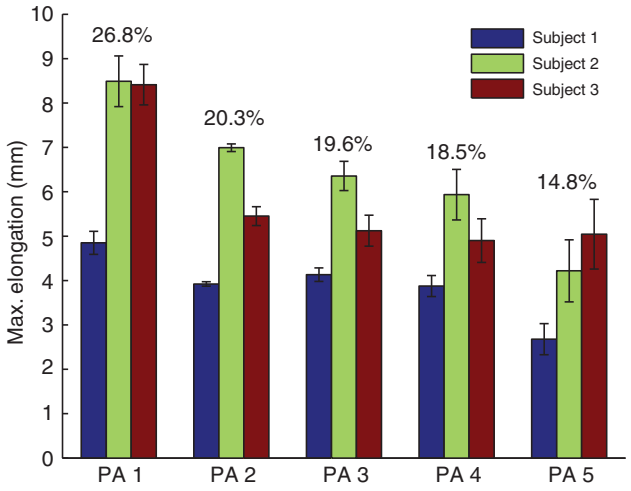

Fig. 9. Means, over five trials, of the maximum elongation in each PA slip (PA 1=medial; PA 5=lateral) for the three subjects during normal walking. The percentage values show the mean, over the three subjects, of the total tension distribution among the five slips.

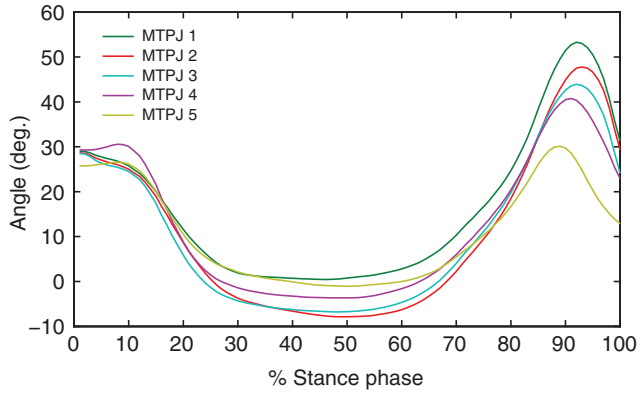

Fig. 10. Intersubject mean temporal profiles, over 15 trials, of the dorsiflexion angle at each MTPJ (MTPJ 1=medial; MTPJ 5=lateral) during normalized stance phase duration.

DISCUSSION

To the best of our knowledge this is the first attempt to reproduce the mechanics of the windlass mechanism in a full 3D model during the stance phase duration of barefoot walking. The temporal loading pattern of the PA (Fig. 8) was very similar to that measured by Erdemir et al. (Erdemir et al., 2004) using cadaveric feet loaded by a gait simulator. In contrast to their finding, however, in this study the PA appeared to be pre-loaded at heel-strike. It seems sensible to assume that some tension may be present in the PA at early stance phase. The simultaneous action of the ankle dorsiflexors and toe extensors, which prevent foot-slap and dorsiflex the toes at the MTPJ, and the plantarflexion moment applied to the calcaneus by the vertical ground reaction forces could account for some pre-stretching of the PA. A MTPJ dorsiflexion angle of about 30 deg. was measured for the three subjects thus confirming the action of the toe dorsiflexors at and prior to heel-strike (Table 4).

Table 3. The resting length (mm) of each plantar aponeurosis slip (PA 1=medial; PA 5=lateral) for each subject when the foot is in neutral position

PA slip	Subject 1	Subject 2	Subject 3	Mean±s.d.
PA 1	154	152	162	156.0±5.3
PA 2	152	154	156	154.0±2.0
PA 3	145	145	153	147.6±4.6
PA 4	140	142	147	143.0±3.6
PA 5	133	135	141	136.3±4.2

Indeed, a recent study has proposed that early stance preloading of the PA may be beneficial to propulsion during walking (Pataky et al., 2008). While the present study strongly suggests that such preloading exists, without further experimental and/or modelling studies, we can only speculate as to the possible advantages of such preloading. Loading the PA at heel-strike is likely to reduce the crimp present in unloaded collagenous tissues (Butler et al., 1978), thereby resulting in earlier arch stiffening and helping to ensure that, as the propulsive phase begins, a greater proportion of force is transferred by the foot to the ground.

Furthermore the detailed kinematics and anatomical description of the windlass mechanism made it possible to estimate the elongation of the five slips of the PA during the whole duration of stance. For all three subjects the medial slip of the PA was the most stretched and the three central slips showed similar patterns of elongation and maximum tension. With the exception of subject 3, whose lateral-slip elongation was comparable to that of the three central slips, the lateral slip was the least stretched (Fig. 9).

From heel-strike to about 30% of the stance phase the length of the PA was rather constant (see Fig. 8). After a peak at heel-strike, the action of tibialis anterior and of toe extensors decreases (Winter and Yack, 1987), and the toes plantarflex, to achieve full contact with the ground, and thus relax the PA. PA elongation lasted from 30% of stance until midstance, as the body weight was borne fully above the longitudinal arch. After midstance, a sharper increase in PA elongation occurred, with a peak at about 80% of stance. The push-off phase is of course characterized by the action of the powerful ankle plantarflexors pulling on the calcaneus *via* the Achilles' tendon. Through the windlass mechanism the PA slips are elongated, being constrained to wrap around the MHs, while the toes, now firmly planted on the ground, dorsiflex at the MTPJs.

The maximum strains recorded for each PA slip in each subject, that is the ratio between maximum elongation and resting length

Table 4. Means, over five trials, of the metatarsophalangeal joint (MTPJ) dorsiflexion angles (deg.) at heel-strike (HS) and at push-off (PO) for the three subjects

	Subject 1		Subject 2		Subject 3		Mean±s.d.	
	HS	PO	HS	PO	HS	PO	HS	PO
MTPJ 1	34±1	53±1	34±1	54±3	20±2	58±3	29±8	54±3
MTPJ 2	38±2	52±1	33±1	51±3	15±2	44±2	29±12	49±5
MTPJ 3	36±2	48±1	31±2	43±5	20±6	44±2	29±8	44±2
MTPJ 4	41±2	43±2	32±1	45±6	21±1	41±2	31±10	42±2
MTPJ 5	39±2	34±3	21±1	26±5	22±2	39±3	27±10	32±7

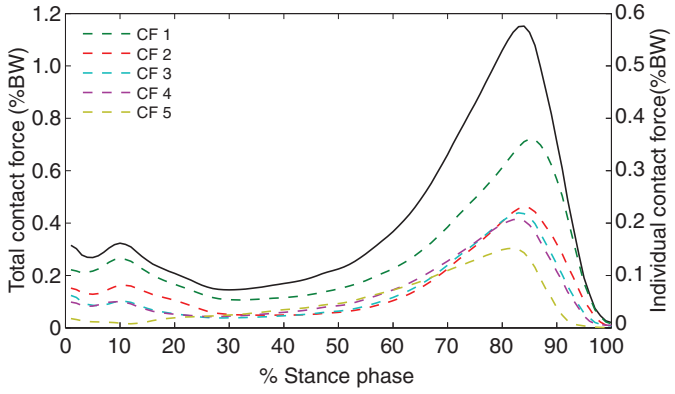

Fig. 11. Dashed curves represent the intersubject mean temporal profiles, over 15 trials, of the vertical component of the contact force at each metatarsal head (CF 1=medial; CF 5=lateral) during normalized stance phase duration. The solid curve is the total vertical contact force, the sum of the contact forces at each metatarsal head. Vertical axes of different scales have been employed to better visualize the individual contact forces (right axis) and the total contact force (left axis).

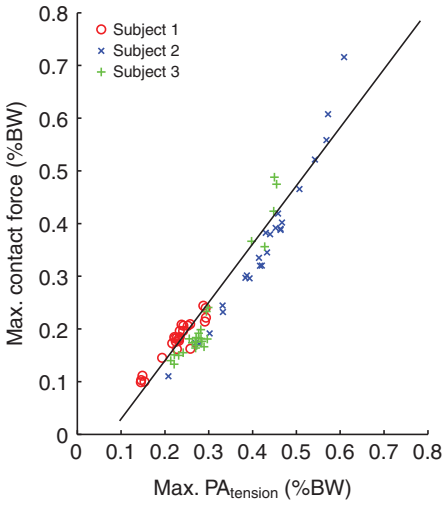

Fig. 12. Correlation plot between maximum tension exerted in each slip of the PA for each subject at each trial (for a total of 75 points) and resultant maximum contact force (CF in Fig. 7) exerted on each metatarsal head.

(Table 3), ranged between 3.5% and 6%, less than those reported by Gefen (Gefen, 2003) on the basis of radiographic fluoroscopy measurements on two subjects (around 12%) but in accordance with *in vitro* cadaveric studies which measured strain of up to 6.5% in the PA (Kogler et al., 1999). In another *in vitro* study (Carlson et al., 2000) the combination of MTPJ dorsiflexion and Achilles' tendon tension caused a maximum strain in the PA of 3.5%. This seems to further support the validity of the current dynamic model.

The maximum $PA_{tension}$, summed across all five slips, was approximately 1.5 BW (averaged across subjects). This was higher than that measured by Erdemir and colleagues (Erdemir et al., 2004) of about 1 BW, but lower than 1.9 BW estimated by Giddins and colleagues (Giddins et al., 2000). A possible explanation for these differences, in addition to the different methodologies employed in these studies, might be related to the adopted estimate of the PA stiffness, determined from mechanical tests on cadaveric feet (Kitaoka et al., 1994). The common mean value of PA stiffness used for all three subjects (203.7 N mm^{-1}) is already affected by significant variance (50 N mm^{-1}) which could imply significant differences in the mechanical properties of the PA tissue among different subjects. Lower maximum tensions in the PA would have been obtained by adopting Gefen's (Gefen, 2003) stiffness value of 170±45 N mm^{-1}. However, Kitaoka's value was adopted in this study as Gefen's value was derived through indirect measurement (fluoroscopy) of a much smaller sample. Moreover the assumption of linear elastic behaviour is an approximation of the actual material properties of the PA (Ker et al., 1987). As already mentioned above, the collagen in the PA tissue could be responsible for a certain degree of crimp, a phenomenon characterizing the stress–strain relationship of collagen-containing tissues such as tendons and ligaments (Butler et al., 1978). As a consequence of crimp, the tension in the tissue is low until the strain has passed a certain threshold (toe-region). For these reasons the elongation and therefore the maximum tension exerted in the PA, as predicted by this model, may have been slightly overestimated.

Fig. 12 reveals a good linear relationship between maximal $PA_{tension}$ and the contact force applied to the MH (Figs 7 and 11). While expected from pulley mechanics, when coupled with the estimated magnitude of the $PA_{tension}$ of 1.5 BW, this finding suggests that the windlass mechanism may be important in maintaining MTPJ integrity. If our interpretation of the mechanism is correct, then one would predict decreased MTPJ integrity with reduced and/or absent $PA_{tension}$.

This hypothesis finds support in a study by Sharkey et al. (Sharkey et al., 1999) who measured a shift of pressure, from toes to the MH, in cadaveric feet, when bands of the PA were sequentially released. In the same study a significant increase was reported in strain and bending in the second metatarsal, probably also affecting all metatarsals to some degree. An increase in the dorsiflexion of the

Table 5. Location (x_o,y_o, mm) of the MTPJ centres relative to the MTPJ reference frame and axis orientation (α_o,β_o; deg.) for each MTPJ (MTPJ 1=medial; MTPJ 5=lateral) for the three subjects as computed by the optimization analysis, based on one set of kinematics data

		Subject 1	Subject 2	Subject 3	Mean±s.d.
MTPJ 1	x	9	6	–3	4±6
	y	–7	1	–3	–3±4
	α	–8	–15	–11	–11±4
	β	–26	–27	–31	–28±3
MTPJ 2	x	–11	–11	–13	–12±1
	y	–17	–9	–10	–12±4
	α	–14	–20	–16	–17±3
	β	–33	–25	–26	–28±4
MTPJ 3	x	–11	–9	–12	–11±2
	y	–14	–5	–12	–10±5
	α	16	3	–6	4±11
	β	25	10	–8	9±17
MTPJ 4	x	–13	5	–9	–6±9
	y	–13	7	–13	–6±12
	α	9	2	17	9±8
	β	18	25	20	21±4
MTPJ 5	x	1	2	2	2±0
	y	–10	–6	–12	–9±3
	α	3	–5	–15	–6±9
	β	–10	0	0	–3±6

Positive rotation angles are eversion and abduction in the frontal and transverse planes, respectively.

first metatarsal has also been measured by Harton et al. (Harton et al., 2002) in patients who had undergone plantar fascioctomy. From the diagram in Fig. 7 it is possible to see how the PA acts to support the vertical forces on the forefoot, and, through the insertion on the plantar aspect of the proximal phalanx, the horizontal component of the tension in the PA acts to pull the proximal phalanx back towards the MH, exerting a plantarflexion moment on the metatarsals which helps to counterbalance the dorsiflexion moment due to vertical ground reaction forces. Therefore the posterior shift of pressure measured in the cited *in vitro* studies following release of the PA appears to be a consequence of an unbalanced force distribution in the forefoot, where the release of the PA would prevent proper support of the MTPJ and decrease the plantarflexion moment applied to the metatarsals through the PA insertion at the proximal phalanges.

As shown by Gibbon and Long (Gibbon and Long, 1999), ultrasound imaging can thus be successfully used to identify the PA origin. Here the combination of sonography and stereophotogrammetry has been used to estimate the 3D location of the origin of the PA in relation to three bony landmarks on the calcaneus. Sonography has again been applied to measure the approximate cephalic radius of the metatarsals. The mean intersubject values are well in accordance with the range of values measured by Largey and colleagues (Largey et al., 2007) on a larger set of bones using CT scanning.

If medial and lateral MH motion is adequately described, the relative motion of the central MHs is less well tracked by the chosen marker set. Magnetic resonance studies of a large group of volunteers have shown statistical differences in the vertical displacement of the second to fourth MH, compared with the first and fifth MH, when changing from a supine position to a position requiring weight bearing by the forefoot (Weishaupt et al., 2002). This could lead to underestimation of the elongation of the three central 'springs' of the PA running underneath these MHs.

The optimization analysis located the axes of the MTPJs near the geometric centre of the MHs (see Table 5). Although this result has been supported at least for non-pathological first rays (Shereff et al., 1986) no publications have addressed this subject for the lateral MTPJs. The maximum dorsiflexion angles of the MTPJs at push-off (Table 4) were within the anatomical range of motion (65 deg.) and decreased from medial to lateral. This was in accordance with normal foot kinematics at push-off, and a probable consequence of the lateral metatarsals lifting off the ground sooner than the first ray, in the propulsive phase (Root et al., 1977).

Intrinsic torsion of the metatarsals has been measured through CT scanning on cadaveric feet (Largey et al., 2007), and shows that the anatomical orientation of the MHs is not parallel to the ground, but rather slightly inverted or everted. The use of non-invasive sonographic imaging in this study did not allow assessment of the degree of inversion/eversion of the MHs of each subject: therefore the cylinders modelling the MHs were represented as parallel to the ground when the foot is in neutral position, and this is clearly a simplification. However, a sensitivity analysis run on this parameter has shown that this approximation affects PA elongation only minimally.

By demonstrating that the windlass mechanism results in early stance-phase loading of the PA, and linking this effect to the radius of the MH, this study also raises interesting evolutionary issues meriting further systematic study. The MHs of chimpanzees and probably other non-human great apes are dorsoventrally shallower than those of humans (Susman and Brain, 1988) [discussed by Aiello and Dean (Aiello and Dean, 1990)] and thus must have a smaller radius. It follows that in their occasional bipedalism the early stance-phase preloading of the PA seen in this study would either not occur or be relatively low. This might in part account for the tail-off in vertical ground reaction forces which differentiates bipedal walking of all other great apes (chimpanzees, bonobos, gorillas and orang-utans) from that of humans (Crompton et al., 2008).

Finally, although data from more subjects would increase the statistical significance of the current results, we must highlight that the three current subjects all showed very similar trends. Furthermore, the intensive nature of the current data collection procedure prohibited us from collecting a larger sample of data; small samples are typical of biomechanical testing of this nature (Gefen, 2003; Giddins et al., 2000). Regardless, the current results should be considered with reference to the limited number of subjects employed in the study.

Conclusions

Sonography and manual biometry have enabled a biorealistic representation of the elements relevant to the analysis of the windlass mechanism, and stereophotogrammetry has enabled us to analyse their *in vivo* dynamics. Preloading of the PA in early stance and the role of the PA in sustaining the MTPJ in late stance have been highlighted. For the first time it has been possible to estimate the distribution of tension in the PA between its five longitudinal slips. The maximum strain in the PA slips decreased from medial to lateral, confirming the role of the PA in sustaining the medial longitudinal arch. These results are novel and emphasize both the importance and complexity of PA dynamics during barefoot walking.

APPENDIX

MTPJs: design optimization approach

The location and the orientation of the five hinge joints, in local reference frames, modelling the MTPJs were identified by means of optimization. The reference frame of the first MTPJ had its origin in (PM_x–l, $FMH2_y$–(R+r), PM_z) and the x-axis belonged to the saggital plane through PM and FMH2 (pointing anteriorly), where: PM_x and PM_z are the x- and z-coordinates of the marker on the proximal phalanx, respectively; $FMH2_y$ is the y-coordinate of the marker on the head of the first metatarsal; R and r are the radii of the metatarsal head (Table 2) and of the reflective marker (3.5 mm), respectively; and l is the proximal phalanx length. The origins of the reference frames of the lateral MTPJs were established according to the convention described above by replacing PM with the marker on the proximal phalanx articulating at that MTPJ (e.g. SPH for the MTPJ of the second toe) and by estimating the y-coordinate of the head of the metatarsal concerned through linear interpolation between $FMH2_y$ and VMH_y, where VMH_y is the y-coordinate of the marker on the fifth metatarsal head (see Figs 4 and 6).

The (x,y) coordinates of the centre of each MTPJ and the axis orientation angle α in the coronal plane, coincident with the yz plane of the joint reference frame, and the axis orientation angle β in the transverse plane, coincident with the xz plane of the joint reference frame, were parameterized. When (x,y)=(0,0) and (α,β)=(0 deg.,0 deg.) the MTPJ rotation axis is coincident with the z-axis of the joint reference frame. This was the MTPJ location at model construction, which was close to the geometric centre of each MH and represented the initial conditions for the optimization analysis.

For each MTPJ, the trajectories of the four markers on the metatarsus and of the marker on the proximal phalanx of the toe during one walking trial were used as input. The optimization

problem was set using the four parameters of each MTPJ axis as independent variables and the mean-squared error between the recorded *in vivo* marker kinematics and their counterparts on the multisegment model as the objective function.

At each time frame t of the dynamic analysis the error function f was computed as the sum of the 3D distances between the markers' trajectories ($\mathbf{MA_i}$) and the computed trajectories ($\mathbf{P_i}$), for i=1,..,5, function of the 5 degrees-of-freedom constraint applied to the segments by the hinge joint. Therefore, for each MTPJ, the objective of the optimization analysis was to find the four values (x_o,y_o,α_o,β_o) that minimized the root mean square (r.m.s.) value of f in the time interval from heel-strike (HS) to toe-off (TO) using one set of walking-kinematics data for each subject (Eqn A1):

$$\text{r.m.s.}\left[\sum_{i=1}^{n}\left|\mathbf{MA_i}(t)-\mathbf{P_i}(x,y,\alpha,\beta,t)\right|\right]_{\text{HS}}^{\text{TO}}, \qquad \text{(A1)}$$

where $\mathbf{MA_i}$ is the (3×1) position vector of the ith motion agent (at time t) and $\mathbf{P_i}$ is the (3×1) position vector of its driven counterpart as computed by the ADAMS solver. The 'motion agents' are small spheres attached to the driven segments *via* six degrees-of-freedom spring-damper elements. The motion agents were constrained to follow the motion of the 12 reflective markers as recorded during the kinematic analysis, after the motion had been filtered and imported into the model as splines. In order to take into account only the displacements around the MTPJ rotation axis, the error at the toe marker was established to be the projection of the distance between the imposed and driven trajectories onto the plane perpendicular to the MTPJ rotation axis passing through the MTPJ centre. The validity of the optimization function was assessed by imposing ideal flexion/extension trajectories (about a fixed axis on the metatarsus) to the toe marker.

ADAMS sequential quadratic programming (OPTDES-SQP) optimization algorithm minimized Eqn A1 for each MTPJ independently.

Table 5 shows the optimal locations of each MTPJ centre and axis orientation relative to the MTPJ reference frame. Good intersubject consistency demonstrates the robustness of the current approach.

LIST OF ABBREVIATIONS

BW	body weight
CF	contact force between PA slip and metatarsal head, vertical component
d	depth of the origin of the plantar aponeurosis
f	error function
HS	heel-strike
l	length of the proximal phalanx
MH	metatarsal head
MTPJ	metatarsophalangeal joint
PA	plantar aponeurosis
PA_o	origin of the plantar aponeurosis
PA_p	projection of PA_o on sole of the foot
$PA_{tension}$	tension exerted by the PA slips
PO	push-off
R	radius of the metatarsal head
r	radius of the reflective marker
r.m.s.	root mean square
RMSE	root mean squared error
TO	toe-off

REFERENCES

Aiello, I. and Dean, C. (1990). An introduction to human evolutionary anatomy. *Am. J. Phys. Anthropol.* **85**, 360-361.

Briggs, P. J. (2005). The structure and function of the foot in relation to injury. *Curr. Orthop.* **19**, 85-93.

Briggs, P. J. and Tansey, P. A. (2001). Active and passive mechanisms in the control of heel supination. *Foot Ankle Surg.* **7**, 131-136.

Butler, D. L., Grood, E. S., Noyes, F. R. and Zernicke, R. F. (1978). Biomechanics of ligaments and tendons. *Exerc. Sport Sci. Rev.* **6**, 125-181.

Carlson, R. E., Fleming, L. L. and Hutton, W. C. (2000). The biomechanical relationship between the tendoachilles, plantar fascia and metatarsophalangeal joint dorsiflexion angle. *Foot Ankle Int.* **21**, 18-25.

Carson, M. C., Harrington, M. E., Thompson, N., O'Connor, J. J. and Theologis, T. N. (2001). Kinematic analysis of a multi-segment foot model for research and clinical applications: a repeatability analysis. *J. Biomech.* **34**, 1299-1307.

Cheung, J. T., Zhang, M. and An, K. N. (2004). Effects of plantar fascia stiffness on the biomechanical responses of the ankle–foot complex. *Clin. Biomech.* (Bristol, Avon) **19**, 839-846.

Crompton, R. H., Vereecke, E. E. and Thorpe, S. K. (2008). Locomotion and posture from the common hominoid ancestor to fully modern hominins, with special reference to the last common panin/hominin ancestor. *J. Anat.* **212**, 501-543.

Erdemir, A., Hamel, A. J., Fauth, A. R., Piazza, S. J. and Sharkey, N. A. (2004). Dynamic loading of the plantar aponeurosis in walking. *J. Bone Joint Surg. Am.* **86A**, 546-552.

Fuller, E. A. (2000). The windlass mechanism of the foot. A mechanical model to explain pathology. *J. Am. Podiatr. Med. Assoc.* **90**, 35-46.

Gefen, A. (2003). The *in vivo* elastic properties of the plantar fascia during the contact phase of walking. *Foot Ankle Int.* **24**, 238-244.

Gibbon, W. W. and Long, G. (1999). Ultrasound of the plantar aponeurosis (fascia). *Skeletal Radiol.* **28**, 21-26.

Giddings, V. L., Beaupre, G. S., Whalen, R. T. and Carter, D. R. (2000). Calcaneal loading during walking and running. *Med. Sci. Sports Exerc.* **32**, 627-634.

Gregg, J., Marks, P., Silberstein, M., Schneider, T. and Kerr, J. (2007). Histologic anatomy of the lesser metatarsophalangeal joint plantar plate. *Surg. Radiol. Anat.* **29**, 141-147.

Harton, F. M., Weiskopf, S. A. and Goecker, R. M. (2002). Sectioning the plantar fascia: effect on first metatarsophalangeal joint motion. *J. Am. Podiatr. Med. Assoc.* **92**, 532-536.

Hicks, J. H. (1954). The mechanics of the foot. II. The plantar aponeurosis and the arch. *J. Anat.* **88**, 25-30.

Jackson, K. M. (1979). Fitting of mathematical functions to biomechanical data. *IEEE Trans. Biomed. Eng.* **26**, 122-124.

Ker, R. F., Bennett, M. B., Bibby, S. R., Kester, R. C. and Alexander, R. M. (1987). The spring in the arch of the human foot. *Nature* **325**, 147-149.

Kitaoka, H. B., Luo, Z. P., Growney, E. S., Berglund, L. J. and An, K. N. (1994). Material properties of the plantar aponeurosis. *Foot Ankle Int.* **15**, 557-560.

Kogler, G. F., Veer, F. B., Solomonidis, S. E. and Paul, J. P. (1999). The influence of medial and lateral placement of orthotic wedges on loading of the plantar aponeurosis. *J. Bone Joint Surg. Am.* **81**, 1403-1413.

Largey, A., Bonnel, F., Canovas, F., Subsol, G., Chemouny, S. and Banegas, F. (2007). Three-dimensional analysis of the intrinsic anatomy of the metatarsal bones. *J Foot Ankle Surg.* **46**, 434-441.

Leardini, A., Benedetti, M. G., Berti, L., Bettinelli, D., Nativo, R. and Giannini, S. (2007). Rear-foot, mid-foot and fore-foot motion during the stance phase of gait. *Gait Posture* **25**, 453-462.

Mohana-Borges, A. V., Theumann, N. H., Pfirrmann, C. W., Chung, C. B., Resnick, D. L. and Trudell, D. J. (2003). Lesser metatarsophalangeal joints: standard MR imaging, MR arthrography, and MR bursography – initial results in 48 cadaveric joints. *Radiology* **227**, 175-182.

Pataky, T. C., Caravaggi, P., Savage, R., Parker, D., Goulermas, J. Y., Sellers, W. I. and Crompton, R. H. (2008). New insights into the plantar pressure correlates of walking speed using pedobarographic statistical parametric mapping (pSPM). *J. Biomech.* **41**, 1987-1994.

Root, M. L., Orien, W. P. and Weed, J. H. (1977). *Normal and Abnormal Function of the Foot.* Los Angeles, CA: Clinical Biomechanics Corporation.

Sharkey, N. A., Donahue, S. W. and Ferris, L. (1999). Biomechanical consequences of plantar fascial release or rupture during gait. Part II: alterations in forefoot loading. *Foot Ankle Int.* **20**, 86-96.

Shereff, M. J., Bejjani, F. J. and Kummer, F. J. (1986). Kinematics of the first metatarsophalangeal joint. *J. Bone Joint Surg. Am.* **68**, 392-398.

Susman, R. L. and Brain, T. M. (1988). New first metatarsal (SKX 5017) from Swartkrans and the gait of Paranthropus robustus. *Am. J. Phys. Anthropol.* **77**, 7-15.

Weishaupt, D., Treiber, K., Jacob, H. A., Kundert, H. P., Hodler, J., Marincek, B. and Zanetti, M. (2002). MR imaging of the forefoot under weight-bearing conditions: position-related changes of the neurovascular bundles and the metatarsal heads in asymptomatic volunteers. *J. Magn. Reson. Imaging* **16**, 75-84.

Winter, D. A. and Yack, H. J. (1987). EMG profiles during normal human walking: stride-to-stride and inter-subject variability. *Electroencephalogr. Clin. Neurophysiol.* **67**, 402-411.